



**HAL**  
open science

## **Sensor array for fetal ECG. part 1 : Simulations.**

Vincent Vigneron, Annabelle Azancot, Christophe Herail, Manuel Schmidt,  
Olivier Sibony, Christian Jutten

### ► **To cite this version:**

Vincent Vigneron, Annabelle Azancot, Christophe Herail, Manuel Schmidt, Olivier Sibony, et al.. Sensor array for fetal ECG. part 1 : Simulations.. 2nd IEEE International Conference on Computational Intelligence in Medical and Healthcare, Jun 2005, Costa da Caparica, Lisbon, Portugal. pp.90-98. hal-00203395

**HAL Id: hal-00203395**

**<https://hal.science/hal-00203395>**

Submitted on 9 Jan 2008

**HAL** is a multi-disciplinary open access archive for the deposit and dissemination of scientific research documents, whether they are published or not. The documents may come from teaching and research institutions in France or abroad, or from public or private research centers.

L'archive ouverte pluridisciplinaire **HAL**, est destinée au dépôt et à la diffusion de documents scientifiques de niveau recherche, publiés ou non, émanant des établissements d'enseignement et de recherche français ou étrangers, des laboratoires publics ou privés.

# SENSOR ARRAY FOR FOETAL ECG. PART 1: SIMULATIONS.

V. VIGNERON<sup>1,2,3</sup>, A. AZANCOT<sup>4</sup>, C. HÉRAIL<sup>2</sup>, M. SCHMIDT<sup>1</sup>, O. SIBONY<sup>4</sup> AND C. JUTTEN<sup>1</sup>

<sup>1</sup>LIS-INPG, France <sup>2</sup>LSC, France <sup>3</sup>MATISSE-SAMOS, France <sup>4</sup>Hôpital R. Debré, France

## ABSTRACT

A fundamental investigation and development for foetal electrocardiogram (fECG) visualization has been carried out in this paper. fECG monitoring is a technique for obtaining important informations about the condition of the foetus during pregnancy and labour by measuring electrical signals generated by the foetal heart as measured from multi-channel potential recordings on the mother body surface. It is shown, in this paper, that the potential electrical field on the mother abdomen can be reconstructed by means of an electrical heart model. Most previous electrical heart models were static, not beating ones. Our study suggests that the beating heart model would provide more accurate simulations.

## 1. FECG MONITORING

Foetal electrocardiogram (FECG) monitoring aims to reduce incidents of unnecessary medical intervention and foetal injury during labor [1, 2] and also to evaluate for the diagnosis of twins, fetal position [3], fetal life [4], congenital heart disease, and asphyxia. Despite this renewed promise, the difficulty of recording abdominal fECG and its questionable yield limite the clinical utility and it was used primarily for research purposes. With this technique, one can obtain fECG signals during pregnancy in a non-invasive manner, but with a weak signal-to-noise (SNR) ratio. In fact, electrodes on the maternal surface pick up the maternal ECG (mECG) and, at a lower voltage, the fECG. Electrodes are also sensitive to other signals, especially electromyographic ones. Therefore, the signal observed on each electrode is a complex signal associated to a superimposition of many sources.

Although volume conduction theory presumes that the whole body is a heterogeneous conductor, the potentials created by the fetal heart are thought to be transmitted to the maternal surface mainly through the umbilical vessel-placenta pathway. Because of the above noted peculiarity of fetal signal transmissions, the recording of the fECG through maternal leads to a waveform that is not affected by changing electrode location. Although the fECG wave configuration does not change when the position of the recording electrodes is changed on the surface of the mother's abdomen, the amplitude of the electrical signal may change. The idealised ECG is illustrated in Figure 1. The shape of the fetal ECG reflects the complex electrical signal - routinely called PQRST waves - conducting within the myocardium (muscular wall of the heart) [5]. Three main characteristics should be obtained from fECG extraction for being useful in early diagnosis of cardiopathologies: fetal heart rate (FHR) [6], amplitudes of different waves, the duration of waves, segments and intervals.

The ECG is a record of the electrical activity of the heart. Its utility stems from the specific changes in the trace caused by various pathologies, which can be measured non invasively by surface electrodes : but, despite signals with higher frequency than the mother heartbeats are identified

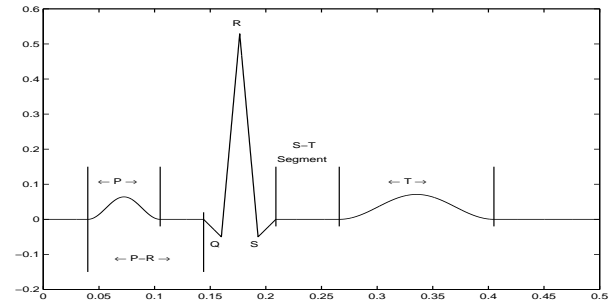


Figure 1: Features of the ECG waveform.

to correspond to the fetal ECG, PQRST waves cannot be easily extracted [7]. The main limitations of noninvasive fECG recording are the low amplitude signal coming from the fetal heart, the high background noise created by the maternal ECG complex, the skin potentials, electromyograms (*i.e.* of womb and diaphragm) and the 50 Hz interference. We propose to use a 3-dimensional simulation model to identify these limitations and evaluate the electric activity on the mother's abdomen.

This paper provide a general framework and make it possible to revisit foetal electrocardiography.

## 2. COMPLETE ELECTRICAL MODEL

### 2.1 A virtual electrical belt

The outputs of the simulator should resemble signals of a belt of electrodes attached to the maternal abdomen. Figure 2 shows the model of the belt where at each crossing of two lines lays one electrode. For most calculations, a number of  $50 \times 50 = 2500$  electrodes was chosen though, in a real application, the number should not exceed  $10 \times 10 = 100$  because the electric field can be easier visualized with a higher number of electrodes. These signals should be used, as described in the part 2 of this article, to develop and validate signal processing algorithms and optimal sensor selection [8]. Simulated signals are needed because the simulator makes it possible to change several parameters such as number of electrodes, neglecting noise or abnormalities of the foetal heart.

The signals provided by the sensors sum the electric fields of several *independent* sources: the maternal heart, the foetal heart, the uterus and the diaphragm. For each of these components, anatomical background is required to derive the equations of the model. These equations were then implemented in *Matlab* and the results will be interpreted. The directions *left* and *right* are always from the view of the patient.

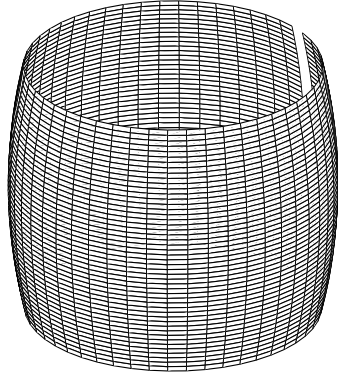


Figure 2: Belt of electrodes.

## 2.2 Bioelectrical model of the heart

### 2.2.1 Anatomical Background

To explain the electric model of the heart - anatomical and bioelectrical phenomena are explained in detail in Malmivuo [9] -, it is necessary to explain the basic mechanism of muscle cells before those principles can be applied for the heart. The heart mainly consists of cardiac muscle which is called *myocardium* and forms four chambers: two atria and two ventricles. To pump the blood out of the chambers, the volume of the chamber is reduced when it is filled. The valves ensure that the blood can exit the chamber only out of one opening. The volume reduction is achieved by contracting the muscle forming the chamber. This contraction is stimulated by *electrical signals* which are generated from the sine node. The sine node consists of self excitatory tissue which means that it does not need any stimulation itself and produces about 70 impulses per minute.

From the sine node the activation impulse propagates through the tissue of the atria and thus causes them to contract (P-Phase). The PR-interval is caused by the slow propagation of the depolarisation through the atrioventricular node (AVN); this allows time for the ventricles to fill. Once the depolarisation reaches the ventricles, conduction must be fast. Ventricular depolarisation is recorded as the QRS-complex. In practice, the Q, R and S waves are not always present.

The heart consists of a large number of muscle cells and each cell produces a dipole field when it is activated (see Fig. 3). But the activation starts at one point and propagates through the tissue which means that the depolarization front forms a layer in the heart. This layer can also be considered as an isochrone. As the two wavefronts of depolarization and repolarization form layers in the heart the model is called *double layer model*. When the electric field is measured from far enough, which holds for ECG applications, all the dipoles of the layer, *i.e.* of all cells activated, can be modelled as *one single dipole*. This dipole, also called *heart vector*, is not moving but its orientation and length change during one heart beat depending on the propagation of the activation layers. Figure 4 displays the orientation and length of the heart vector during several heartbeats.

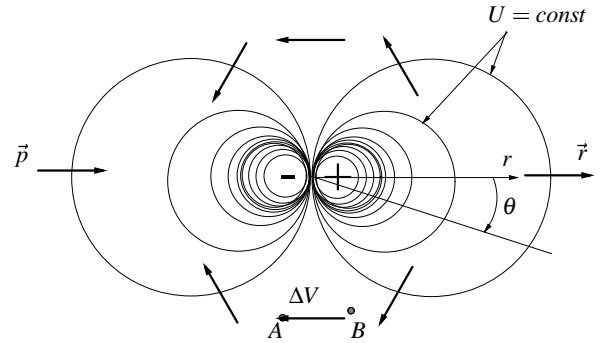


Figure 3: Potential and electric field of a dipole.

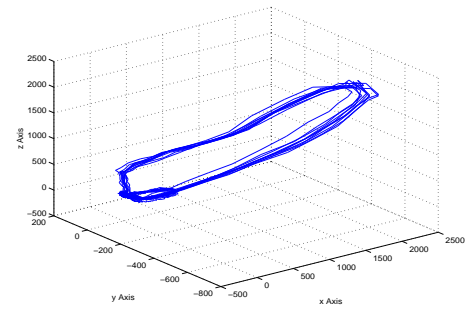


Figure 4: Heart vector during several beats.

In a muscle fiber many cells are connected to each other so that the activation impulse can propagate through the fiber. Altogether there are two wavefronts one after the other propagating through the fiber. Before the first front, the potential in the cell is negative afterwards positive and after the second front negative again. The electric field arising from one wavefront is the same as from a dipole as in the dipole. The potential of the dipole  $U$ , visualized by figure 3, is expressed by

$$U = \frac{1}{4\pi\epsilon_0} \frac{\vec{p} \cdot \vec{r}}{r^3} = \frac{Q}{4\pi\epsilon} \frac{l \cos \theta}{r^2}, \quad (1)$$

where  $r$  is the distance away from the center of the dipole,  $\vec{p}$  the vector dipole moment,  $Q$  the point charge.  $\vec{p} \cdot \vec{r}$  gives the relative orientation of the potential difference  $\Delta V = V_A - V_B$  between two points  $A$  and  $B$ . At the depolarizing front, the dipole points in the direction of the propagation (from “plus” to “minus”) while, at the repolarizing front, the dipole is pointing in the other direction than the propagation.

### 2.2.2 Implementation

The simulator is written in *Matlab* scripts. Three steps can be identified for the simulation of the heart:

1. the coordinates of the electrodes have to be defined,
2. the models of the hearts of mother and foetus have to be generated,
3. the electric field has to be calculated.

The tradeoff, as in most simulation tasks, is between the accuracy and the complexity of the model. In this task, the shape of the maternal abdomen is considered to be formed

by a parabolic function rotated around a middle axis (see Fig.2). Thus, the *cylindric* coordinates of the sensors can be given by

$$s_{\mu,\eta} = \begin{pmatrix} \rho \\ \theta \\ h \end{pmatrix} = \begin{pmatrix} -0.2(H-0.5)^2 + 0.5 \\ \frac{2\pi}{C}\eta \\ \frac{H}{L}\mu \end{pmatrix}, \quad (2)$$

with  $\mu = 1, \dots, L, \eta = 1, \dots, C$  and where  $C$  is the number of sensors on one circle of the same height (column),  $L$  is the number of sensors lying at the same angle (lines),  $H$  is the total height of the belt. In this paper, a hundred-electrodes belt ( $N = C \times L = 100$ ) located around the pregnant woman's abdomen is considered.

### 2.2.3 Generation of the heart model

The difficulty of this task is, that an accurate model of the heart is needed, because the model has to provide the orientation of the heart dipole. This could be achieved by building a model out of many single muscle cells and their interconnections and position in space so that the propagation of the electric impulse is calculated and is the same as found in a real heart. As this approach seemed too complex and time consuming, a file of previously recorded vector ECG data was imported. This template file consisted of  $x, y$  and  $z$  coordinates of the tip of the heart vector<sup>1</sup>, while the base of the heart vector was located at  $(0,0,0)$ . The recorded data was filtered to suppress high frequency noise and the heart rate was adjusted by resampling the data. The data imported was recorded at a sampling frequency of 500Hz and the heart rate was 70 beats/min. If the sampling frequency is considered to be 1KHz, the heart rate would be 35 beats/min. Thus by changing the sample rate and still considering that it is 500Hz, the effective heart rate can be adjusted to any value. With this model, one maternal and one foetal heart were built, while the heart rate of the foetus is about twice the maternal one and the mother's amplitude is ten times higher than the amplitude of the foetus.

### 2.2.4 Calculating the field

With the coordinates of the sensors and the location and orientation of the two heart dipoles, the electric field at the sensors is calculated. For this purpose at every time step the electric field of every sensor is calculated using equation (1). The resulting field takes into account the two hearts - mother and foetus -, the diaphragm and the uterus; it is plotted in figure 5 in a grid sensor representation for a foetus QRS duration.

The equivalent mapping in 3 dimensions is given by Fig. 6: the green dot is the location of the foetal heart and the green line indicates the actual orientation and length of the foetal heart vector. The blue dot and the blue line correspond to the maternal heart location and vector respectively. In this simulation the maternal and foetal heart are placed near to each other in order to visualize the fields better, but, for realistic simulations, the positions of the hearts followed realistic geometrical data.

<sup>1</sup>This draws attention to the selection of the appropriate file. If the person from which the measurement comes from had some anatomic anomalies, the simulator computes output data for a pathologic case. A physician has to judge whether the template vector ECG data is valid data or not.

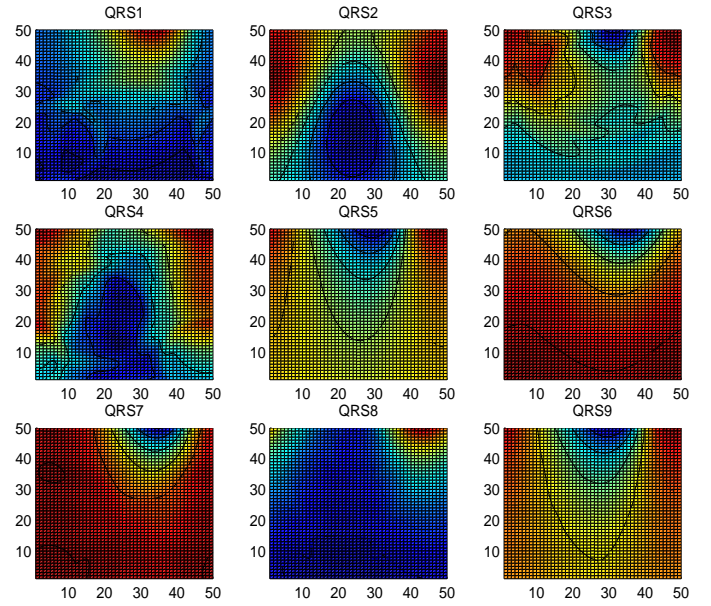


Figure 5: Snapshots of the electric field taking into account the two hearts (fetus and mother), the diaphragm and the uterus, for the PQRST duration.

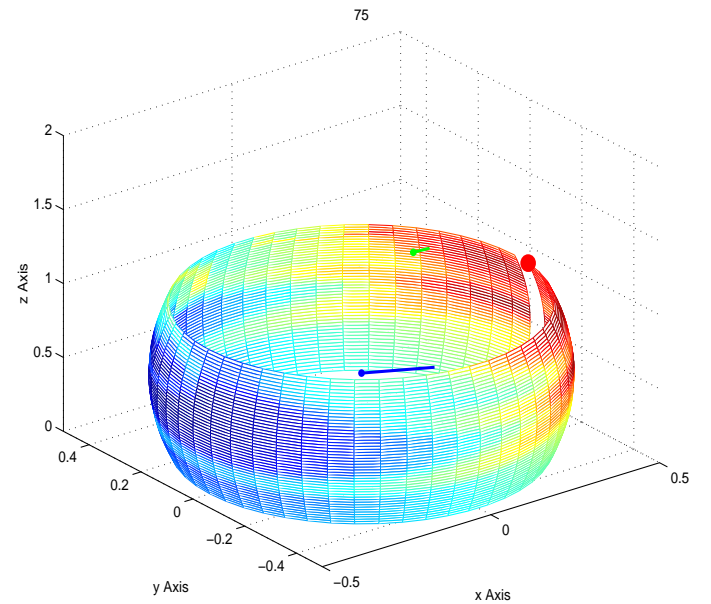


Figure 6: 2 dimensional of the electric field from the two hearts.

### 2.2.5 Volume Conductor

During calculation of the cardiac field, some simplifications were made which will be discussed in the following. The first effect neglected is the time the signal needs to propagate from the source to the electrodes. The signal arrives later at those electrodes which are farther away from the source. This time shift  $\Delta t$  is calculated by  $\Delta t = \frac{\Delta x}{v}$  with distance  $\Delta x$  and speed  $v$ . For  $\Delta x = 1$  m and  $v = 2 \cdot 10^8$  m/s the result is  $\Delta t = 5 \cdot 10^{-9}$  s = 5 ns. This time shift could be detected using sampling rates above 200 MHz which is far beyond the projected sampling rate for this application. Thus the signals at the electrodes are modelled arriving *at the same time*.

Concerning a second effect, it is assumed, that each layer of tissue is *homogenous, isotropic* and without dynamic elements. This means that the signal of one source is attenuated only depending on the distance between this source and the electrode. An exact procedure would be to find a transfer function for the channel between each source and each electrode which models the attenuation of different directions and frequencies at different locations. It was decided, that the enhancement is not worth the effort for finding the appropriate transfer function.

The third issue is the following: during the calculation of the electrical field at the surface, the structure of the body is not regarded to. The existence of different layers consisting of fat, muscle tissue, amniotic fluid and others was neglected though each layer has different bioelectrical properties like, for instance, conductivity which is discussed in [10]. The reason for that is the following, still under the assumption of homogenous, isotropic tissue layers: By inserting an additional layer of tissue into the simulator, the signal of the heart will be more attenuated than without the layer. Due to the assumptions mentioned above, this attenuation is the same for every electrode. Hence it is the same effect as simulating the sources inside this layer with a lower amplitude. Thus this simplification only leads to an inaccurate relation between the amplitudes of the different sources which is the same for every electrode and a more accurate simulation would not lead to better results as the relation of the amplitudes of the sources themselves are also not known exactly and can be chosen arbitrarily.

## 2.3 Biomedical model of the uterus

### 2.3.1 Anatomical Background

The uterus mainly consists of smooth muscles, the myometrium, which belongs to the autonomous nervous system, *i.e.* it cannot be controlled *voluntarily*. The uterus of a non pregnant woman is pear shaped and measures about 7,5 cm in length, 5 cm in breadth, at its upper part, and nearly 2,5 cm in thickness. It is positioned in the abdomen of the woman. Additional anatomical information can be found in [11]. During gestation the uterus enlarges as the foetus grows in the uterus. The task of the myometrium is to press the foetus out of the maternal abdomen during delivery. But this activity has to be avoided before the appropriate age of gestation which is achieved by a complex mixture of chemical and physical effects. Some aspects of the complex mechanisms in the uterine tissue are described by [12] and [13].

### 2.3.2 Generation of the uterus model

The bioelectrical properties of the uterus are derived from [14]. The activation of muscle cells in the myometrium

starts at one point of spontaneous depolarization which will be called *pacemaker* [15]. From this point spreads a front of activation with the shape of an *ellipse*. In the whole uterus, more than one pacemaker could be active at the same time with the effect that more than one ellipse is spreading over the muscle tissue but every pacemaker will only once activate an ellipse, though more than one pacemaker could exist for the same location but with different starting time. The measurements for three active pacemakers of which one has started recently are displayed in Fig. 7.

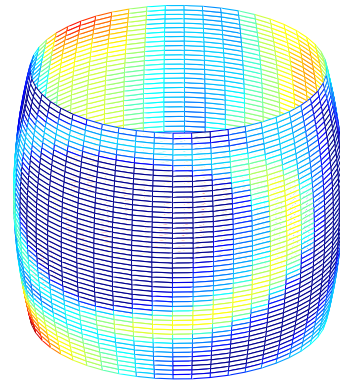


Figure 7: Electric field of the uterus with three active pacemakers

Due to the fact that the tissue is inhomogeneous and unidirectional, blocks exist in the tissue, circular re-entries of activation zones are possible. But as re-entries occur in the minority of the activations and they are difficult to implement into the simulator, it was decided that, during the simulations, occur none of them. Hence they are not further explained.

### 2.3.3 Implementation

One way to calculate the electrical field emitted by the uterus could be to model the muscle cells the same way as modelled in the heart. But while simulating the heart, one fundamental fact was assumed that is not valid in this case. Now, the observing electrodes are not far enough away from the sources to model the many dipole sources as one dipole. Or in other words, the sources are far less concentrated in space. Hence, the electric dipole field has to be computed for every single muscle cell at every electrode. As this is far too complex and time consuming, another implementation was found which will be explained in the following.

It is assumed that the uterus is placed near the electrodes. The uterus is imaginary divided into as many partitions as electrodes are used so that each electrode is located over the center of one partition, which is illustrated by figure 8. When one partition of the uterus is activated, it can only be observed at the electrode of that partition. The contribution to the field at the other electrodes is neglected. Further, the distance and direction between the dipole of the uterus muscle and the electrode is constant and thus, it is not necessary to compute the electric field. It is sufficient to add a constant value to the potential measured at one electrode if

the partition is activated. This is achieved by the following calculation using the notations defined in section 2.2.2.

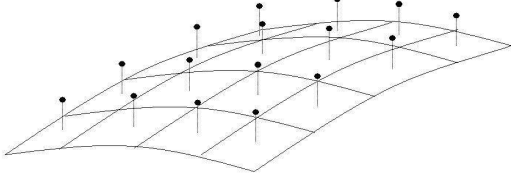


Figure 8: Electrodes over the uterus

For each pacemaker exists one entry in a  $n \times 3$  pacemaker matrix

$$\mathbf{P} = \begin{pmatrix} t_{0,0} & \mu_0 & \eta_0 \\ t_{0,1} & \mu_1 & \eta_1 \\ \vdots & \vdots & \vdots \\ t_{0,n} & \mu_n & \eta_n \end{pmatrix}, \quad (3)$$

where  $n$  is the number of pacemakers which start their spreading ellipse of activation at time  $t_0$  at line  $\mu$  and column  $\eta$ . In the following, the matrices  $\mathbf{A}_k$ ,  $\mathbf{D}_k$ ,  $\mathbf{F}_k$  and  $\mathbf{F}$  have the dimension  $L \times C$ , with  $k = 1, \dots, n$  being the index of the pacemaker. Let  $a_{ij,k}$  be the element in line  $i$  and column  $j$  of the matrix  $\mathbf{A}_k$ .

The matrix  $\mathbf{D}_k$ , which stores the distances from every electrode to the pacemaker  $k$ , is computed. At every time step  $t$ , the activation matrix  $\mathbf{A}_k$  is

$$\mathbf{A}_k = \frac{\mathbf{D}_k}{t - t_{0,k}}, \quad (4)$$

is computed. This is shown by Table 1, for an ideal example of two dimensions and one pacemaker which is located at the left side of the figure: a propagating **1** can be realized which reflects the propagation of the impulse. Later it will be explained how a division by zero is avoided.

$D :$	1	2	3	4	5	6	7	8	9	10
$t = t_0 + 1, A = \frac{D}{1}$	<b>1</b>	2	3	4	5	6	7	8	9	10
$t = t_0 + 2, A = \frac{D}{2}$	0.5	<b>1</b>	1.5	2	2.5	3	3.5	4	4.5	5
			$\vdots$							
$t = t_0 + 5, A = \frac{D}{5}$	0.2	0.4	0.6	0.8	<b>1</b>	1.2	1.4	1.6	1.8	2

Table 1: Impulse propagation in the uterus.

The values of the matrix  $\mathbf{A}_k$  which are out of a certain interval, e.g.  $[0.8, 1.2]$  are considered to be *inactive*, and, thus, set to zero. The values which lie in that interval - i.e. are *active*- are transformed by a *pulse forming function* :

$$f_{ij,k} = -100(a_{ij,k} - 0.8)(a_{ij,k} - 1.2). \quad (5)$$

This function, together with the zeroing of inactive partitions, is plotted in figure 9.

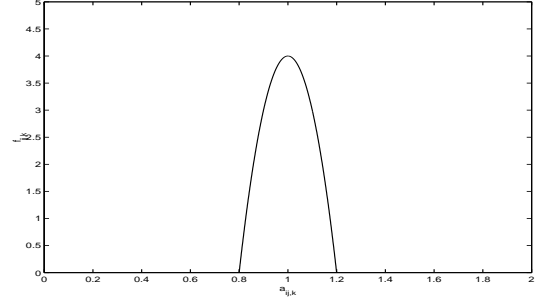


Figure 9: Impulse of one activated uterus partition.

The resulting matrix  $\mathbf{F}_k$  stores the electric field for all electrodes deriving from the ellipse of activated tissue of pacemaker  $k$  at one time step. To put it in a nutshell, those electrodes measure uterus activity which have the same distance to the pacemaker while this distance enlarges in time. Furthermore this distance differs with direction so that the result is an ellipse with changeable length of the axes. In other words the activation propagates faster in one direction than in the other. Finally all field matrices are summed,

$$\mathbf{F} = \mathbf{F}_1 + \mathbf{F}_2 + \dots + \mathbf{F}_n, \quad (6)$$

to get the field represented by  $\mathbf{F}$  for all spreading ellipses.

This procedure had to be changed due to the following reasons: it is not appropriate to choose the positions of the pacemakers before the simulation because, if the number of pacemakers should be augmented from  $n = 20$  to  $n = 30$ , the whole matrix  $\mathbf{P}$  has to be changed if the pacemakers should be equally distributed in time and space. Additionally, the computing complexity enlarges with the simulated time because, for a longer time, more pacemakers are needed and every pacemaker is calculated even though it is not yet activated or even though its ellipse has spread already over the whole uterus. Furthermore it should be possible that pacemakers are added randomly. For those purposes, the following alternative procedure was developed. The matrix  $\mathbf{P}$  does not contain *all* pacemakers but *only* those which are actually *active*. Hence  $\mathbf{P} = \mathbf{0}_{n,3}$  holds for  $t = 0$ . At every time  $t_i$ , there are two possibilities that a pacemaker is added to  $\mathbf{P}$ :

- first, if, in the set of predefined pacemakers, is one entry with  $t_{0,k} = t_i$ , then this pacemaker is appended to  $\mathbf{P}$ .
- second, when a random number, which is generated every time step, is greater than a predefined threshold  $\alpha$ , a pacemaker is appended to  $\mathbf{P}$  with  $t_{0,k} = t_i$  and random coordinates. The generation rate of pacemakers can be controlled by changing the threshold value  $\alpha$ . Furthermore, by changing the random distribution of the coordinates, regions of a high generation rate could be modelled.

If the ellipse of one pacemaker has spread over the whole uterus this pacemaker should be eliminated out of  $\mathbf{P}$ . This is achieved by finding the *maximal* value in  $\mathbf{F}_k$ . If that value is below a predefined limit, then the pacemaker  $k$  is deleted out of  $\mathbf{P}$ . It is also possible, with this proceeding, to delete pacemakers before they have spread over the whole uterus. If an attenuation factor proportional to the time is added to equation (5), the pulse gets weaker while

it spreads. When its amplitude is below the limit, the pacemaker is deleted.

#### 2.3.4 Interpretation

Until now the modelling of the uterus as a bioelectric source was not necessary, as the measurement of the activity of special regions of the uterus was of little use for diagnosis in opposition to the measurement of the heart, where the knowledge of conductivity and activation characteristics of special regions are vital for an appropriate diagnosis. Thus the evaluation of the simulated data is not easy as real measurements are not common and hence not accessible to compare them with the simulated signals. This drawback is faced by the flexibility of the simulator because the properties of uterus activation change completely when certain parameters are changed in the simulator.

### 2.4 Biomedical model of the diaphragm

#### 2.4.1 Anatomical Background

The diaphragm is a sheet shaped muscle at the bottom of the chest cavity thus, over the uterus. Its task is to inflate and to deflate the lungs to let them exchange oxygen and carbon dioxide with the surrounding air. More detailed information can be found in [16].

Diaphragm electromyogram (dEMG) signal is generated by different respiratory muscles signals that overlap in time and frequency domain. Diaphragm muscles are controlled by train of electric firings, sent by the central nervous system (see Fig. 10) via moto-neurons (MN). Each phrenic nerve trunk extends bilaterally to the thoracic surface of the diaphragm where it separates into 3 branches, each of which enters the diaphragm in close proximity. A motor unit (MU) consists of a MN and the muscle fibers that it innervates. The electrical activity of a firing MU (also called motor unit action potential - MUAP) can be detected by intramuscular or surface electrodes. The dEMG signal obtained results from the temporal and spatial summation of asynchronously firing MUAP trains during spontaneous muscle contractions.

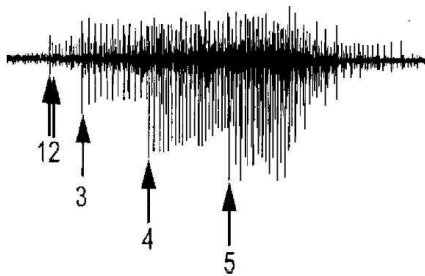


Figure 10: Train of electric firings detected by intramuscular recordings showing the superimposed activity of several MUs.

Usually, dEMG is detected by intramuscular recordings, obtained by placing needle electrodes inside the muscle. MUAP waveforms are in fact sharp enough to identify single MUs. Recent advances open the possibilities of acquisition of surface electromyograms with multi-electrode pick-ups placed on arbitrary muscles groups (see Fig. 11).

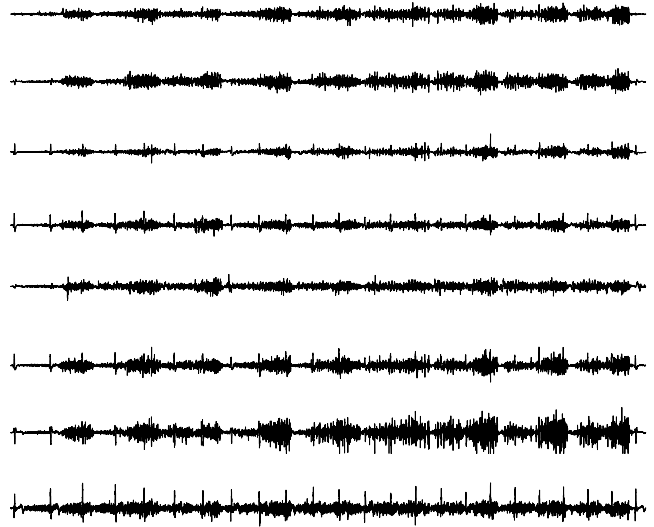


Figure 11: Example of signals obtained from 8 surface electrodes distributed randomly on the thorax.

#### 2.4.2 Generation of the bioelectrical model

A number of studies investigation EMG generator have already been carried out [17, 18]. One paper that deals with this topic is presented under Aldrich *et al.* [19]. We developed a dEMG generator based on Disselhorst-Kulg *et al.*'s model [20]. Using this model, we produced dEMG signals of any duration. These signals were composed of the same number of motor units and firing at 20 firings/second. The model is mainly the same as for the heart muscle, only with a different shape and activation characteristic. While the tissue of the heart is not activated at the same time, the cells of the diaphragm are synchronized to ensure a smooth contraction of the whole muscle. Thus it is not necessary to model the field as a dipole with changing direction but as a dipole with fixed direction and changing amplitude. Since the diaphragm is not a concentrated muscle, it is modelled not by only one, but by several dipoles distributed randomly and, as the diaphragm moves, the position of the dipoles also change with the respiration rate which is about 0.3 Hz.

#### 2.4.3 Implementation

The implementation is quite simple as it only consists of a number of dipoles, *e.g.* 3, 5, 8 or 10, which are located over the uterus. The exact position as well as the amplitude can change over time. According to new information about the way this muscle tissue emits an electric field [21], these properties can be adopted.

#### 2.4.4 Interpretation

Evaluating the model of the diaphragm apply similar things as for the uterus in section 2.3.4. Exact information is rarely available as this information yield little help for diagnosis.

### 3. APPRAISAL OF THE INTEGRATED MODEL

There are important differences between the simulated signals and this model. The first difference is that the hearts

are emitting their electric field not homogeneously in all directions. The fields are generated by dipoles with fixed position but changing direction. Thus, regarding only one heart, the signals of two neighbouring electrodes are not only of different amplitude but also shifted in time depending on the position of the electrodes.

In addition, the signal is not only *shifted* but also its *shape* is changed. Simplifying, it can be described as like the different peaks of the PQRST wave have different changes in amplitudes for different direction. In other words, switching from one electrode to a neighbouring electrode, the Q peak could be higher while the R peaks is lower.

Note that the signals of the simulator are computed as fields emitted from one point in the body with characteristics of dipoles. Except the signal emitted by the uterus. As described in section 2.3, this source is not concentrated at one point, but distributed over the whole grid. Moreover, the uterus is not emitting the same field at every position. This leads to the drawback that the signal of the uterus is *different* for different electrodes.

It should be examined if the various different tissues surrounding the fetus don't influence the electrical field significantly. It was assumed that the dynamic elements for instance are negligible, but that assumption is not enough proved to be valid. Thus further versions of the simulator might contain models for the propagation of electric fields in the body tissue.

The model for the uterus is derived from the rat uterus assuming that the uterus of the rat and the uterus of a human are similar. One way to evaluate the model could be the use of invasive electrodes with pregnant animals and thus measure the muscle activity directly.

The model of the diaphragm seems to be a "reasonable" approximation of the reality. Measurements with surface electrodes of the electrical activity of the diaphragm (see Fig.11) have been favourably compared with *simulated* ones.

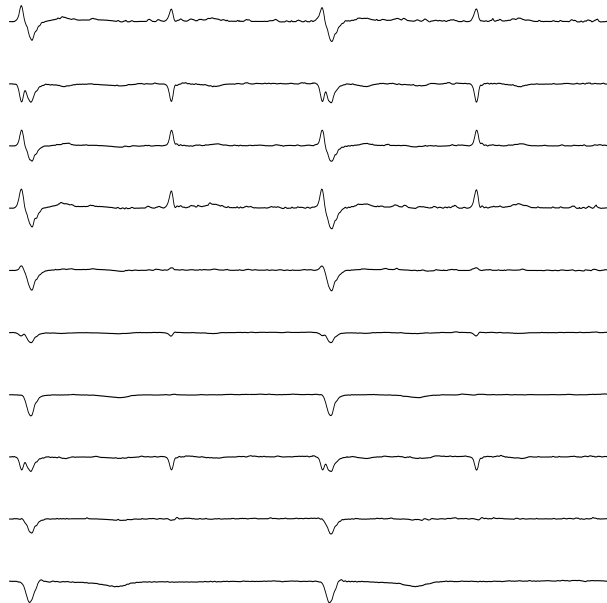


Figure 12: Example of simulated recordings from 10 electrodes, chosen randomly on the sensor array.

Though the simulator is already used to provide data on which we can test processing methods for optimal sensor selection or to make "real time" extraction of fECG<sup>2</sup>. Figure 12 provides an example of simulated recordings from 10 electrodes, chosen randomly on the sensor array; figure 13 plots the 3-dimensional potential field jointly with an electrode recording, chosen randomly on the grid.

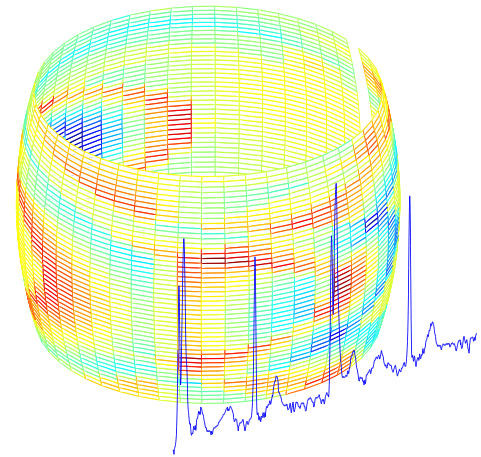


Figure 13: 3-dimensional potential field and an electrode recording provided by the simulator.

#### 4. CONCLUSION AND FURTHER WORKS

For monitoring the foetal state of health, several approaches such as cardiocography, foetal blood sampling, foetal magnetocardiography are available, which differ by the physical and physiological phenomena used and the way they are measured. On the contrar, the aim of this work is a model based reasoning approach, capable (i) to help with the development and the validation of signal processing algorithms, (ii) to improve the knowledge gained on the properties of the signals such as how the field of the rotation dipole behaves or which cardiac abnormalities are detectable, which questions have to be answered.

This work provides basic information for future researchers. Theoretic research in the field of source separation and in the field of sensor selection was made by using the simulator and results are presented in the second part.

#### REFERENCES

- [1] C.N. Smyth. Electrocardiography of the fetus. *The Lancet*, pages 1124–1126, 1953.
- [2] R.S. Fowler and V. D. Finlay. *The fetal circulation*, chapter The electrocardiogram of the neonate, pages 72–80. Addison-Wesley, 1978.

<sup>2</sup>For this purpose, a graphical user interface was written for the simulator and various parameters can be easily changed.



- [3] H. Lilja, K. Larlsson, K. Lindecrantz, S.S. Ratnam, A.S. Thavarasah, and K.G. Rosen. Microprocessor based waveform analysis of the fetal electrocardiogram during labor. *Int. J. Gynecol. Obstet.*, 30:109–116, 1989.
- [4] K.G. Rosen and R. Luziett. Intrapartum fetal monitoring: basis and current developments. *Prenat. Neonatal. Med.*, pages 1–14, 2001.
- [5] C. Widmark, T. Jansson, R. Lindecrantz, and K.G. Rosen. Ecg waveform short term heart rate variability and plasma catecholamine concentrations in response to hypoxia in intra uterine growth retarded guinea pig fetuses. *J. Develop. Physiol.*, 15:109–116, 1995.
- [6] O. Sibony, P. Fouillot, M. Benaoudia, A. Benhalla, J-F. Oury, and P. Blot. Quantification of the fetal heart rate variability by spectral analysis of fetal well-being an fetal distress. *European Journal of Obstetrics and Gynecology and Reproductive Biology*, 54:103–108, 1994.
- [7] V. Vigneron, A. Paraschiv-Ionescu, A. Azancot, C. Jutten, and O. Sibony. Fetal electrocardiogram extraction based on non-stationary ICA and wavelet denoising. In *7th IEEE International Symposium on Signal Processing and its applications*, Paris, July 2003.
- [8] F. Vrins, M. Verleysen, and C. Jutten. *Independent Component Analysis and Blind Signal Separation*, volume LNCS 3195 of *Lectures Notes in Computer Science*, chapter Sensor array and electrode selection for non-invasive fetal electrocardiogram. Extraction by independent Component Analysis, pages 1017–1025. Springer, 2004.
- [9] J. Malmivuo. *Bioelectromagnetism*. Oxford University Press, 1995.
- [10] J.G. Stinstra and M.J. Peters. The influence of fe-toabdominal volume conduction on the fetal MCG. In *Biomag*, pages 831–834, 2000.
- [11] H. Gray. *Anatomy of the human body*. lea & febiger, 2000.
- [12] B.N. Sanborn, C. Yue, W. Wang, and K.L. Dodge. G protein signalling pathways in myometrium: Affecting the balance between contraction and relaxation. *Reviews of Reproduction*, 3(196), 1998.
- [13] S.C. Riley, R. Leask, J.R. Selkirk, R.W. Kelly, A.N. Brooks, and D.C. Howe. Increase in 15-hydroxyprostaglandin dehydrogenase activity in the ovine placentome at parturition and effect of oestrogen. *Journal of Reproduction and Fertility*, 119(329), 2000.
- [14] W.J.E.P. Lammers. Circulating excitations and re-entry in the pregnant uterus. *Eur J Physiol*, 433:287–293, 1997.
- [15] M. Khalil and Duchêne. Une approche pour la détection fondée sur une somme cumulée dynamique associée à une décomposition multi-échelle. application à l’EMG utérin. In *XVII colloque GRETSI*, pages 1049–1052, 13-17 septembre 1999.
- [16] P. Cluzel, T. Similowski, C. Chartrand-Lefebvre, M. Zelter, J.P. Derenne, and P.A. Grenier. Diaphragm and chestwall: Assessment of the inspiratory pump with MR imaging preliminary observations. *Radiology*, page 215:574, 2000.
- [17] P.Y. Guméry, S. Meignen, H. Roux-Buisson, E. Aithocine, and P. Lévy. Reconstruction process of the berkner transform: Application to scale range determination in a genioglossal EMG reflex time-scale detector,. In *Proceedings of 25th Annu. IEEE-EMBS Conf*, pages 2606–2609, Cancun, September 2003.
- [18] S. Karlsson, J. Yu, and M. Akay. Time-frequency analysis of myoelectric signals during dynamic contractions. *IEEE Transactions on Biomedical Engineering*, 47(2):228–238, 2000.
- [19] T.K. Aldrich, C. Sinderby, K.D. McKenzie, M. Estenne, and S.C. Gandevia. Electrophysiologic techniques for the assessment of respiratory muscle function. *Am. J. Respir. Crit. Care Med.*, 166:548–558, 2002.
- [20] C. Disselhorst-Kulg, J. Silny, and G. Rau. Estimation of the relationship between the noninvasively detected activity of single motor units and their characteristic pathological changes by modelling. *Jour. of electromyography and kinesiology*, 8:323–335, 1998.
- [21] A. Merlo, D. Farina, and R. Merletti. A fast and reliable technique for muscle activity detection from surface EMG signals. *IEEE Trans. Biomed. Eng.*, 50:316–323, 2003.